Tuijin Jishu/Journal of Propulsion Technology
ISSN: 1001-4055
Vol. 45 No. 3 (2024)

Optimizing Load Flexibility in Coal-Fired Power Plants through Combined High-Temperature Thermal Energy Storage

Mr. P. Rajesh[1*], Dr. D. R. Srinivasan[2], K. Sridhar[3], Dr. Sunil Vasant Prayagi[4]

[1]Research and development, Xpertmindz Innovative Solutions Private Limited, Kuzhithurai, Tamil Nadu, India.*

[1]Email: rajeshkannan.mt@gmail.com*

[2]Assistant Professor, Department of Mechanical Engineering, JNTUA College Of Engineering, Anantapur, Andhra Pradesh, India

[3]Professor, Department of Mechanical engineering, Kakatiya Institute of Technology & Science, Warangal, Telangana, India.

[4]Professor and Registrar, Department of Mechanical Engineering, Yeshwantrao Chavan college of Engineering, Nagpur, India.

Abstract- A novel method is proposed for increasing load flexibility in coal-fired power plants (CFPP) by combining an extra thermodynamic cycle with high-temperature thermal energy storage (HTTES) system. The purpose of the study is to determine if it is feasible to integrate HTTES into a standard CFPP's steam-water cycle and evaluate the possibility of obtaining high round-trip efficiency through this integration. A detailed analysis of the thermal system and operation mode of a CFPP with HTTES is provided. A subcritical CFPP model is developed for performance assessment and discussion. The proposed system is implemented using MATLAB, and the results demonstrate improved load flexibility for conventional CFPPs. While the primary unit operates at rated capacity, additional net power generation is possible. This study contributes comprehensive insights into utilizing high-temperature thermal energy storage (TES) for enhancing load flexibility in CFPPs.

Keywords: *Thermal energy, Energy storage system, Coal fired power plant, heat, thermodynamic, mass of flow, efficiency, temperature, load flexibility.*

1. Introduction

CFPPs remain pivotal in meeting global electricity demands, despite the growing imperative for cleaner and more flexible energy systems in light of climate change and resource depletion [1]. However, the integration of renewable energy sources (RESs) into the grid presents challenges because of their intermittent nature, leading to curtailment and inefficiencies [2, 3]. As such, there is a pressing need to enhance the flexibility and efficiency of CFPPs to accommodate the increasing penetration of RES while ensuring a reliable power supply [4-6].

Over the years, efforts have been made to mitigate the limitations of CFPPs by incorporating energy storage technologies [7-9]. As a potential means of improving CFPP flexibility by storing extra thermal energy during low demand and using it at peak demand, TES has emerged as a feasible approach [10, 11]. Previous strategies, such as integrating TES into the boiler system, have shown promise but have encountered operational challenges and low efficiency, particularly when addressing short-term load fluctuations [12-14].

In this work, we propose a new method to optimize load flexibility in CFPPs through the combination ofHTTES systems [15]. By employing an extra thermodynamic cycle, our approach aims to overcome the limitations of previous TES implementations and maximize the use of stored thermal-energy [16]. Specifically, We examine whether integrating HTTES devices into a steam-water cycle of CFPP is feasible and evaluate the

possible for achieving high round-trip efficiency [17]. A detailed analysis and simulation using MATLAB aims to provide insights into the performance benefits and technical challenges associated with this innovative approach [18, 19].

This research represents a significant step towards enhancing the operational flexibility and sustainability of CFPPs in the context of evolving energy systems [20, 21]. By optimizing load flexibility through the integration of HTTES systems, we aim to contribute to the efficient combination of RESs while ensuring the reliable operation of coal-fired power plants [22]. The results of this study have significance for researchers, policymakers, and operators of power plants who are attempting to tackle the difficulties involved in making the shift to a more robust and sustainable energy system [23].

1.1. Contribution Statement:

- Proposes a novel approach for enhancing load flexibility in CFPPs through HTTES integration, offering a fresh perspective on addressing operational challenges.
- Conducts a comprehensive feasibility study to assess the viability of HTTES integration into CFPPs, supported by rigorous modeling and simulation techniques.
- Demonstrates significant improvements in efficiency and flexibility with HTTES integration, achieving a thermal storage efficiency of 46.9% and enhancing conventional efficiency to 42.5%.
- Provides valuable insights for future research and implementation efforts, guiding further exploration and refinement of HTTES integration in CFPPs.

Overall, this research contributes to advancing CFPP optimization and offers actionable insights for industry practitioners and policymakers aiming for a more sustainable energy future. The remaining manuscript is presented below: sec. 2 clarifies recent research work, sec. 2.1 depicts the background, sec. 3 clarifies configurations of CPFF that integrate HTTES, sec. 4 describes the result and discussion, and sec. 5 completes the paper.

2. Recent Research Work: A Brief Review

Numerous researches have earlier presented on the literature was based on improving coal-fired power plants' load flexibility. Some works were reviewed here,

Zhu et al. [24] have presented the creation of a dynamic model for direct air-cooling condensers that is connected with a 600 MWe CFPP to look into how power and heat interact throughout the DACC-CFPP under several load as well as environmental circumstances. To consider the effects of crosswind, the condenser was exhibited as a one-dimensional multi-section structure, and a thorough turbine-feed water heater system model was created to link the power plant and direct air-cooling condenser.

To increase the load-flexibility of CFPP, Cao et al. [25] have developed a novel approach for incorporating HTTES through an extra thermodynamic-cycle. It aims to determine whether the steam-water cycle of traditional CFPP may incorporate an additional cycle aided by HTTES and to examine how HTTES integration can result in high round-trip efficiency.

The time-varying and specific boiler-heat storage features have been defined and suggested by Wang et al. [26], which has boosted the flexibility of power-plant. For a double-reheat power plant, dynamic simulation and control models were created and tested. The principal parameters were derived by employing a stepwise regression algorithm, specific characteristics of the boiler's heat storage as well as represent the time-varying.

Through GSE programming, Wang et al. [27] have developed a powerful reproduction models and temperature control schemes of a double-reheat boiler, which were later approved to comprehend the heat storage change rule of law. A new mechanism that takes into account changes in heat storage was developed. The flexibility of unique and further developed control techniques was analyzed. An inventive main steam-extraction scheme for modifying power-output during low load periods has been proposed by Wei et al. [28].

Molten salts and phase-change materials were utilized to store the sensible as well as latent-heat of the removed steam throughout the load lessening process. The heat that had been saved was used once more throughout the load-raising process to heat the feed and condensate waters.

For the purpose of sizing and improving the working of TES units in combined heat and power (CHP) plants, Benalcazar. [29] have created a novel decision support approach.

The created method provides three steps depends on the characterization of the thermal load, they were, (1) producing an estimate of the storage capacity, (2) enhances the application of the approach by making it possible to analyze the hourly operation of the CHP plant with thermal storage, (3) evaluates the long-term financial effect of upgrading the CHP plant with a heat-storage option.

Liu et al. [30] have developed simple steam ejector-based heat power decoupling systems that are both inexpensive and highly effective. Three brand-new CHP systems with built-in ejectors were developed, while some system parameters were adjusted. Comparisons were also made between the energy consumption traits and heat power decoupling capabilities of the three reformatted systems [31-35].

2.1. Background of Recent Research Work

The review of the latest research reveals the importance of adding high thermal energy storage to increase the load flexibility of CFPP. [36] Incredible vapor sensible- and latent-heat are present in the separated steam at a higher temperature. There is a pinch point temperature differential and a significant latent heat of steam condensation if sensible material is used to store all of the extracted steam's heat.

In response, the following objectives of this work are set forth: (1) provide a unique way to employ the thermal energy stored in a conventional CFPP with high quality and efficiency by integrating the high temperature TES into it; (2) assess the viability of incorporating an HTTES into a thermal power plant's water-steam cycle with a high-parameter added thermodynamic-cycle [37] and (3) assess the system's performance. These above-mentioned drawbacks are motivated us to do this work.

3. Configurations of CFPP by Integrating HTTES

A novel type of CFPP integration with HTTES also referred to as a high temperature thermal energy storage assisted CFPP is proposed in the current work [38]. Fig. 1 displays Configuration of Thermal system for HTTES-assisted CFPP [39]. The two primary subsystems that make up the whole power-generation scheme are the conventional CFPP and the additional HTTES-aided power unit [40].

A typical subcritical coal-fired power plant uses the original thermodynamic cycle; these units can be CHP units, straight condensing steam units, or they can include several regeneration phases in addition to a single reheat [41]. The fact that a sub-critical thermal power unit's boiler is a drum boiler is an important factor. A supercritical Rankine cycle is an additional thermodynamic cycle, and an HTTES system serves as its heat source.

The real and additional cycles can interchange mass and energy thanks to the original plant's boiler drum, which links the two power units [42-46].

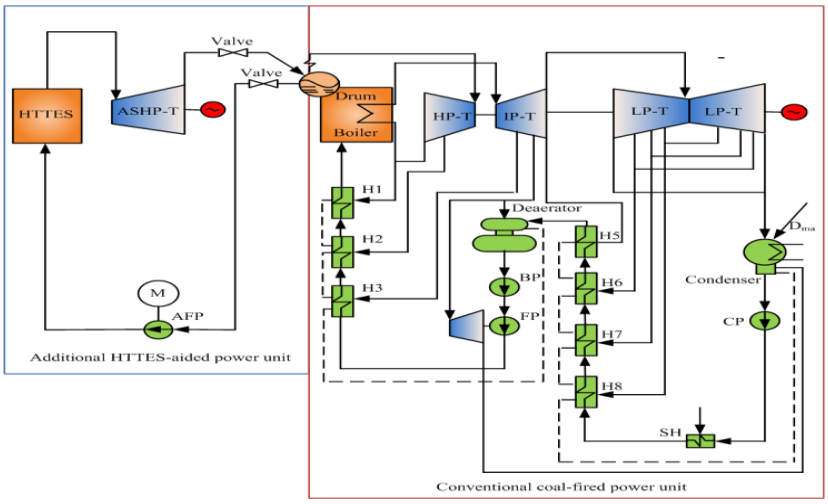

Fig 1: Configuration of Thermal system for HTTES-assisted CFPP

3.1. Modeling of High Temperature Thermal ESS

Latent TES, sensible TES, and thermochemical TES are the 3 primary types of TES systems that are employed in practice. Each of them has benefits and drawbacks. [47] The choice of a TES system is influenced by factors such as operational conditions, economic viability, and the desired storage duration (diurnal or seasonal). [48] The steam generator, electric heating devices, HTTES tank, and other auxiliary equipment are all associated in an HTTES system.

A crucial factor is the TES system's size. Here is a straightforward example that provides an initial sizing of thermal energy storage for a certain power mandate so that you can get a clear idea of its size. The thermal storage system is a single-tank thermo cline system. The heat storage medium, which may function between 300 and 700 °C, is a combination of 45 weight percent LiCl and 55 weight percent KCl.

The thermal storage tank has a fundamental volume of around 4000 m3, assuming a charging-power of 100 MW as well as an 8-hour charging period. Although the fact that this has significant impact on the entire approach's operational viability, our intention in this study is not to take into consideration any particular HTTES system. As a result, we do not take into consideration any particular HTTES scheme.

The expected output temperature of high temperature TES system to remain constant throughout the discharge process to make the analysis process simpler. The system's heat source is a crucial component in the consolidation of TES system into a thermal power plant. Previous research work has shown that heat is charged in thermal ESS in two ways: electric boiler heating and steam extraction heating.

The steam of high-temperature is taken from an appropriate place in the power plant's water-steam form and sent via heat exchangers mounted in a thermal energy storage structure to store heat at off-peak hours for the steam-extraction system. As the name implies, the materials in the TES system are heated by an electric boiler while in the electric boiler mode. Due to the substantial loss of exergy that occurs at the process of electric heat, the former has a higher thermodynamic efficiency than the latter [49].

Given the power plant's operational security, however, the maximal storage capacity for the steam-extraction method is subject to a number of limitations [50]. Additionally, the extracted steam's characteristics, particularly its pressure, directly affect the temperature of the thermal energy that has been stored [51]. Instead, a more flexible approach to responding to changes in grid load demand can be used using the electric boiler mode [52].

The high-temperature electric-boiler that serves as the heat-source in the current analysis is powered by the output power of the original device. It is supposed that for the high temperature thermal energy storage systems,

the charging-time is t_{chg} as well as the discharging-time is t_{dischg}. The high temperature TES system is idle state (normal-mode) during other times.

Supposing that the high temperature TES system's charging power is P_{chg}, the net cost of stored thermal energy is given the following Eq. (1):

$$\overline{Q}_{chg} = 3600\, P_{chg} t_{chg} \tag{1}$$

For a variety of theoretical and technical reasons, the thermal energy that has been stored cannot be completely released and used again during the discharge process. Therefore, the effective discharge efficiency η_{TES} is typically introduced to measure the quantity of available energy. It is the proportion of overall thermal-energy stored to useable energy that can be improved from the high temperature TES system.

In order to express the thermal energy that is available and reused in the additional and initial cycles Eq. (2),

$$\overline{Q}_{dischg} = \overline{Q}_{chg} \eta_{TES} \tag{2}$$

3.2. Additional Thermodynamic-Cycle Modeling

A unit of super or ultra-super critical is a further cycle of thermodynamics. The mechanical-power used by the feed-pump set, or compression work, is expressed as follows Eq. (3):

$$w_{p,adl} = h_7 - h_5 = \frac{(h_{7s} - h_5)}{\eta_{p,adl}} \tag{3}$$

here the water-feed pump's isentropic efficiency denotes $\eta_{p,adl}$.

Compressed water is subsequently fed into the high-temperature TES system. Where, heat $q_{1,adl}$ is supplied to the water to produce steam is given below Eq. (4):

$$q_{1,adl} = h_g - h_7 \tag{4}$$

The other high-pressure turbine produces useful work. The extra high-temperature thermodynamic-cycle's turbine work (mechanical power) can be stated as follows Eq. (5):

$$w_{T,adl} = \eta_{ri,adl}(h_g - h_{9s}) \tag{5}$$

here the relative internal effectiveness of turbine denotes $\eta_{ri,adl}$; if the development method of the turbine is isentropic, h_{9s} refers to turbine exhaust specific-enthalpy.

Heat $q_{2,adl}$ defines unrestricted in boiler-drum of innovative plant to close the cycle, and the fluid then returns to the first position 5 that may be written by Eq. (6):

$$q_{2,adl} = h_9 - h_5 \tag{6}$$

In this manner, the ratio of net work to additional heat, or the true thermal efficiency η_{adl}, can be calculated as Eq. (7):

$$\eta_{adl} = \frac{w_{T,adl} - w_{p,adl}}{q_{1,adl}} = 1 - \frac{q_{2,adl}}{q_{1,adl}} \tag{7}$$

Lastly, the total power for an extra thermodynamic-cycle may be determined as Eq. (8),

$$P_{adl} = \frac{D_0 \alpha_{adl} (w_{T,adl} \eta_{m,adl} \eta_{g,adl} - w_{p,adl})}{3600} \tag{8}$$

here the additional-cycle's starting steam mass flow rate fraction signifies $\alpha_{adl} = D_{adl} / D_0$;the original thermodynamic cycle's initial mass flow rate of steam denotes D_0 ; (this also represents the drum water extraction mass flow rate fraction at point 5). The functioning time for the discharge procedure (or the discharge-time), according to the energy balance t_{dischg} can be represented by Eq. (9):

$$t_{dischg} = \frac{\overline{Q}_{dischg}}{q_{1,adl} D_0 \alpha_{adl}} \tag{9}$$

3.3. Analysis of thermal-system performance

The study above shows that even when the prior thermal power plant is running at its rated condition, the high temperature TES-assisted CFPP's peak-valley load regulation range is reliant on the characteristics of the new thermal power unit. The total output power of the apparatus might be as low as $P_e - P_{chg}$ While its operation in the power absorption mode, in which the high-temperature TES system stores energy power.

When it operates in power-regeneration-mode, the thermal-energy has been stored, which is used for thermal power through an additional unit, as well as the whole unit's output-power extends to $P_e + P_{adl}$. The sum of electricity produced for the total power-system inside an operating-loop (such as discharging and charging) can be calculated as follows Eq. (10):

$$W_{cp,loop} = 3600[(P_e + P_{adl}) t_{dischg} + (P_e - P_{chg}) t_{chg}] \tag{10}$$

Let's now concentrate on how much heat is used in a single operating cycle.

During an operational cycle, the initial thermal power unit's boiler provides all of heat needed for generation. The initial thermal-power unit (TPU) is fully operates in the power-absorbing mode while operating at full capacity and with the boiler's thermal load set at Q_b. Although the thermal-load on the boiler is reduced at power-regeneration, the steam-turbine of initial thermal-power unit continues to operate as intended.

The reason for this is the innovative thermal power unit's boiler drum, which recovers heat from the extra thermodynamic-cycle. Hence, the following is a statement of the boiler's thermal load in power-regeneration method Eq. (11):

$$Q_b' = (1 - \alpha_{adl}) Q_b + \alpha_{adl} (Q_b - D_0 q_{2,adl}) = Q_b - \alpha_{adl} D_0 q_{2,adl} \tag{11}$$

As a result, the entire system's heat consumption for generating inside an operational loop can be determined as follows Eq. (12):

$$\begin{aligned} \overline{Q}_{cp,loop} &= \frac{Q_b - \alpha_{adl} D_0 q_{2,adl}}{\eta_b} t_{dischg} + \frac{Q_b}{\eta_b} t_{chg} \\ &= \frac{Q_b (t_{dischg} + t_{chg}) - \alpha_{adl} D_0 q_{2,adl} t_{dischg}}{\eta_b} \end{aligned} \tag{12}$$

The boiler effectiveness of the initial thermal-power unit is η_b, and it is supposed that η_b remains stable for a range of boiler thermal loads.

As a result, the following formula can be used for calculating the unit-generation effectiveness of the high temperature TES discharging method,

$$\eta_{cp,dischg} = \frac{3600\,(P_e + P_{adl})\eta_b}{Q_b - \alpha_{adl} D_0 q_{2,adl}} \tag{13}$$

Also, within an operational loop, the mean unit generating effectiveness can be calculated as Eq. (14):

$$\eta_{cp,m} = \frac{W_{cp,loop}}{\overline{Q}_{cp,loop}} \tag{14}$$

Substituting Eqn. (1), (2), (9), (10) and (12) into Eqn. (14), it produces:

It can be found from Eq. (15) that charging power of high-temperature TES system P_{chg} , $\eta_{cp,m}$ are mostly based on the efficient discharging of high temperature TES system η_{TES}, and the original steam-parameters (mass flow rate, pressure, and temperature) of the additional-cycle.

3.4. Analyses the use of TES Performance

The round-trip effectiveness of the energy storage power source is a crucial parameter for assessing technological proficiency. It is the ratio of the net cost of electricity consumed during the charging process to the net cost of electricity generated from stored energy. The net cost of energy stored in the high temperature thermal ESS at the mode of power absorption is $\overline{Q}_{chg}$.

At the power-regeneration mode, the thermal energy that has been stored is separated into 2 halves and used successively by the primary thermal-power unit and the secondary thermal-power unit. The total power-output of the extra thermal-power unit is P_{adl}. The power-output of the initial thermal-power unit (P_e) may remain unchanged when the heat load of the boiler decreases because the finish heat of the additional cycle is recycled in the boiler-drum of the initial-cycle $q_{2,adl}$, which is also recycled in the boiler-drum of the initial-cycle.

Assuming that the original thermal power unit's boiler efficiency remains constant under various boiler thermal loads, corresponding boiler thermal-load Q' , equal power-output $P_{e,eq}$, which are measured as

$$P_{e,eq} = P_e \frac{Q'_b}{Q_b} = P_e \frac{Q_b - \alpha_{adl} D_0 q_{2,adl}}{Q_b} \tag{15}$$

Hence, the equal power-output of TES regeneration is represented by Eq. (16):

$$\begin{aligned} P_{adl,eq} &= P_e + P_{adl} - P_{e,eq} \\ &= P_e \frac{D_0 \alpha_{adl} q_{2,adl}}{Q_b} + \frac{D_0 \alpha_{adl} (w_{T,adl} \eta_{m,adl} \eta_{g,adl} - w_{p,adl})}{3600} \\ &= D_0 \alpha_{adl} \left[\frac{P_e q_{2,adl}}{Q_b} + \frac{(w_{T,adl} \eta_{m,adl} \eta_{g,adl} - w_{p,adl})}{3600} \right] \end{aligned} \tag{16}$$

The round-trip effectiveness of the high temperature thermal energy storage-assisted CFPP η_{rt} is computed by Eq. (17):

$$\eta_{rt} = \frac{3600\, P_{adl,eq} t_{dischg}}{\overline{Q}_{chg}} \tag{17}$$

Sub. Eqn. (2), (7)-(9) and (17) into Eq. (18), it produces:

$$\eta_{rt} = \eta_{TES}\left[\frac{\eta_{cp}}{\eta_b}(1-\eta_{adl}) + \frac{(w_{T,adl}\eta_{m,adl}\eta_{g,adl} - w_{p,adl})}{q_{1,adl}}\right] \quad (18)$$

The following represents the round-trip efficacy of storing energy for the high-temperature thermal energy storage-assisted CFPP, presuming disregard for the extra density work cycle.

$$\eta_{rt} = \eta_{TES}\left[\frac{\eta_{cp}}{\eta_b} + \eta_{adl} + \eta_{adl}\left(\eta_{m,adl}\eta_{g,adl} - \frac{\eta_{cp}}{\eta_b}\right)\right] \quad (19)$$

It concludes that from Eq. (19) η_{rt} is mostly based on the actual-discharging effectiveness of the high temperature TES system η_{TES} the real-thermal effectiveness of extra cycle is η_{adl}.

The structural layout and operational plan of HTTES system are η_{TES}. The primary determinants of η_{adl} are the main steam pressure and temperature of the extra thermodynamics cycle.

4. Results and Discussion

Integrating an additional thermodynamic cycle to HTTES, this study proposes a novel approach for improving coal-fired power plants' load flexibility. It aims to determine whether an HTTES-aided extra cycle may be incorporated into the steam-water cycle of traditional CFPP and to investigate whether HTTES integration may lead in high round-trip efficiency. By that time, the novel approach that has been proposed is being used in MATLAB platform and is connected to a number of other current ways.

Fig. 2 shows the analysis of power output and mass flow. Subplot 2(a) shows the variations in power output. The target output starts with 70% at the beginning and decreases to 25% at the time period of 0.7hr. Then it remains constant till the time reaches 4.9hrs. After that it rises to 40%. At the time of 7hrs, the target power output reaches to 90%. The measurement power output starts with 80% and it decreases down to 25% at 1.9 hr. After that it remains constant till 4.9hrs. While the time reaches to 7hrs, the measurement power output reaches to its maximum of 90%.

The simulation power also starts with 80% at the beginning and decreases to 25% at the time of 1.2hrs. Then it remains constant till the time reaches 4.9hrs. After that it starts to increase and reaches to 90% when the time is 7hrs. Subplot 2(b) portrays the variations in mass-flow. The measurement live steam starts with 450kg/s at the beginning and decreases to 50kg/s at the time of 1.2hrs. Then it starts to vary and the variation continues till 4.9hrs.

At the time of 7hrs the steam reaches the maximum mass of flow 600kg/s. Simulation live steam is at 450kg/s mass of flow at the beginning and decreases down to 50kg/s at 1.1hr. Then it remains constant till 4.9hrs. At the end of the cycle the simulation live steam is at 590kg/s mass of flow. Measurement of inlet economizer starts with 450kg/s mass of flow and decreases to 250kg/s at 0.5hr.

At the end of the cycle in 8hr the measurement inlet economizer's mass of flow reaches its maximum of 560kg/s. The simulation inlet economizer's mass of flow reaches its maximum of 50kg/s at the time of 7hr. Fig. 3 shows the comparative of measurement and simulation parameters (a) temperature (b) mass of flow. Subplot 3(a) depicts the temperature variations of measurement and simulation live steam, outlet evaporator, and inlet economizer.

The measurement live steam starts with 540 ºC at the beginning and it slightly varies till the time of 1.2hrs. After that it remains constant up to 4.1hrs. Again the variation continues till the end of the cycle. The simulation live steam starts with 540 ºC and remains constant till 5.5hrs. After that it slightly varies and the variation continues up to 7hrs. Finally, the simulation live steam remains constant at the temperature of 540 ºC from 7 to 8hrs.

The temperature of the measurement outlet evaporator starts with 390 ºC and decreases to 300 ºC at 2hrs. After that it remains constant till the time reaches to 4.9hrs. At the end of the cycle, the measuring outlet evaporator reaches its highest temperature of 390ºC. The simulation output evaporator's temperature rises to 390ºC and then drops to 300ºC after 0.9 hours. Then it remains constant till the time of 4.9hrs.

The measurement inlet economizer starts with 240ºC at the beginning and drops to 200 ºC at 1hr. Then it rises to 240 ºC at the time of 1.1 hr. At the end of the cycle the measurement inlet economizer is at 240 ºC. The differences in mass-flow of the measurement and simulation output circulation pump and injection cooling are shown in Subplot 3(b). The measurement outlet circulation pump starts mass of flow remains constant at 0kg/s from 0 to 1hr.

After that it rises to 125kg/s at the time period of 1.1hr. At the time of 4.4hrs, the mass of flow in measurement outlet circulation pump reaches its peak of 150kg/s. Finally, it drops down to 0kg/s at 5hrs. Simulation outlet circulated pump's mass of flow starts with 0 at the beginning and remains constant up to 0.9hr. At 2hrs the mass of flow increases to 130kg/s and remains constant up to 4.9hrs. The mass of flow in measurement injection cooling starts with 30kg/s at the beginning and decreases to 0kg/s at 1hr.

Then it rises to 0.10kg/s and remains constant up to 5hrs. Finally, the mass of flow ends with 50kg/s. The mass of flow in simulation injection cooling starts with 40kg/s at the beginning and decreases to 10kg/s at 1hr. After it remains constant till the time reaches 5hrs. At the end of the cycle, the mass-flow is 90 kg/s. Fig. 4 portrays comparative of measurement and simulation pressure under the steam accumulator process.

The measured pressure starts with 34 bars at the beginning and rises to 40 bars at the time of 200 sec. At the time of 500 sec the pressure is at 45 bar. At the end of the cycle at 700 sec the pressure reaches the maximum of 47 bars. The simulated pressure is at 34 bar at the beginning and increases to 40 bar at 200 sec. At the end of the cycle, the simulated pressure reaches a maximum of 47.1. Fig. 5 depicts the analysis of firing rate and pressure.

Subplot 5(a) depicts the variations in set point net power, firing rate and net power.

The set point net power starts with 100% at the beginning and remains constant till 0min. After that, at end of the cycle, it increases to 104.2% and remains stable. At end of the cycle, firing rate starts at 100% and remains stable. The net power starts with 100% at the beginning and remains constant upto 0min. Then it rises to 104.2% at the time of 1min and drops to 104% at 23min. Finally, at the end of the cycle, the net power drops to 100%.

Subplot 5(b) depicts the variations of pressure in Ruths storage and pressure extraction to HPP 6. The pressure in Ruths storage starts with 40 bar pressure and at the beginning and remains constant upto 0min. After4 that it drops to 21bar at 40min and remains constant till the end at 60min. The pressure extraction to HPP 6 starts with 20bar at -5min and remains constant till 0min.

Then it rises to 22.5bar at 0.1min and remains the same till 23min. At end of the cycle the pressure is at 20bar. The analysis of mass-flow and valve opening are shown in Fig. 6. Subplot 6(a) depicts the variation of mass flow outlet ruths storage. It starts from -5min with 0kg/s and reaches to the maximum of 60kg/s in 0.1min. After that the value decreases to 49kg/s in 6min. At the time of 21.5min the value is at 48kg/s.

Finally the value drops to 0kg/s at the end of cycle in 60min. Subplot 6(b) depicts the variation of valve opening position which starts with 0% from -5min and increases to 44% at 1min. At end of the cycle, 22min the value is at 100% and remains stable. Fig. 7 portrays the analysis of the mass flow in extraction to HPP 6 in kg/s. The value starts with 49.5kg/s at the beginning and remains constant till 1min. After that it drops to 1kg/s at 2min.

Then the value increases to 10kg/s at 23min. At the time of 60min the mass of flow value is at 49.5kg/s in the end of the cycle. Fig. 8 shows the analysis of set point net power, firing rate and net power in %. The set point net power is at 100% in the beginning and remains constant upto 0 min. After that, at end of the cycle it drops to 95% at 1min and remains stable. The firing rate is at 100% from the beginning and remains constant till 60min in the end of the cycle.

The net power is at 100% at -5min and remains same upto 0min. Then it drops to 94.5% at the time period of 2.5min. In 30min the net power reaches 97%. Finally the net power reaches 99.8% in 60min. The comparison of mass flow storage and valve opening position are shown in Fig. 9. Subplot 9(a) depicts the inlet mass flow ruths storage which starts from -5min with 0kg/s and reaches to the maximum of 60kg/s in 1 min.

After that it decreases to 50kg/s in 4min. In 20min the value is at45kg/s. At end of the cycle the mass-flow drops to 2kg/s. Subplot 9(b) depicts the valve opening position which is 0% in -5min and increases to 55% in 1.5min. After that it decreases to 40% in 8min. Finally, at end of the cycle in 22.5 min it reaches the maximum of 100% and remains stable.

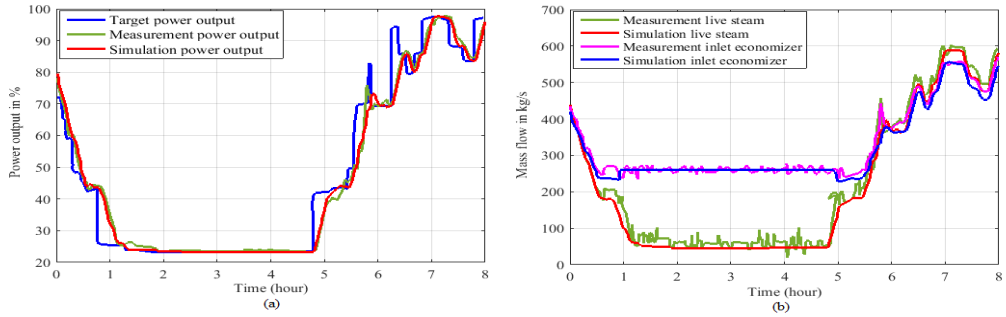

Fig 2: Analysis of (a) power output (b) mass flow

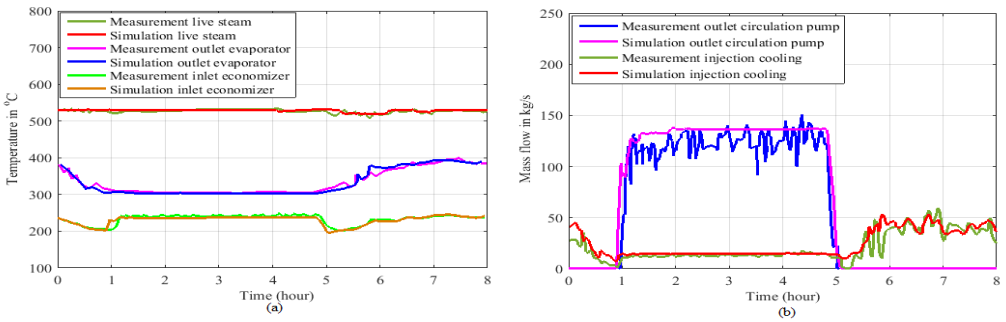

Fig 3: Comparative of measurement and simulation parameters (a) temperature (b) mass of flow

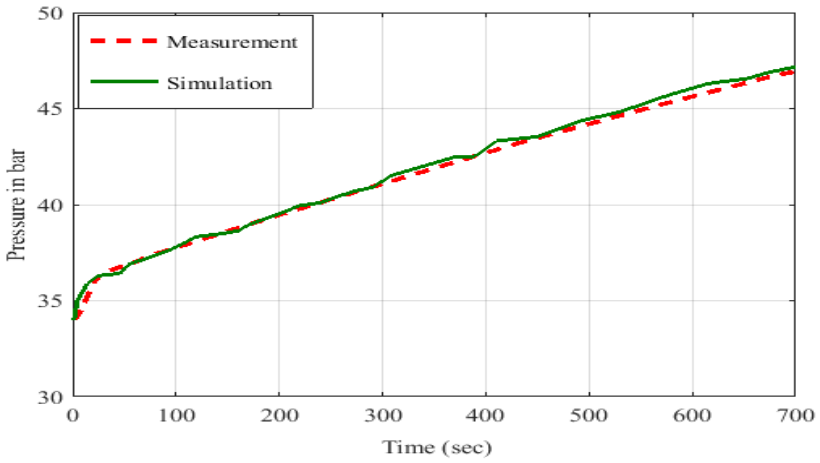

Fig 4: Comparative of measurement and simulation pressure under the steam accumulator process.

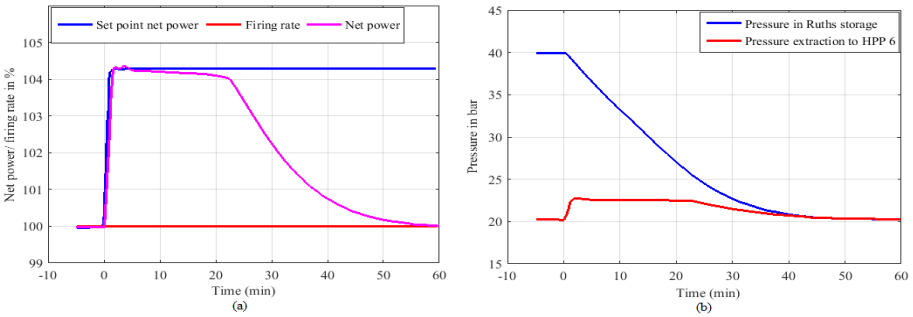

Fig 5: Analysis of (a) firing rate and (b) pressure

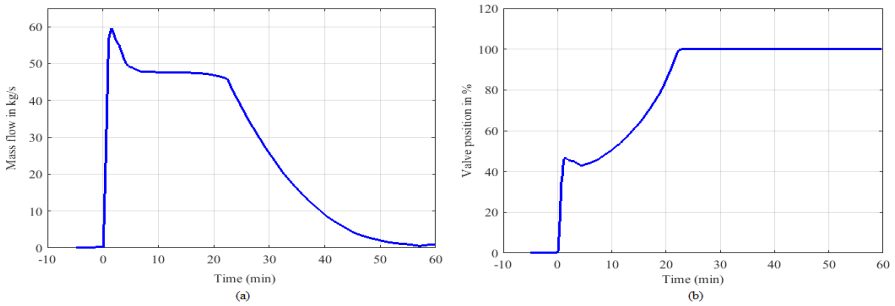

Fig 6: Analysis of (a) mass flow outlet Ruths storage (b) valve opening position

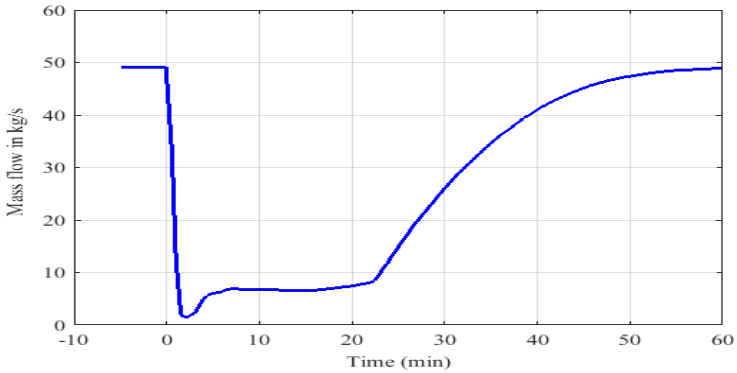

Fig 7: Analysis of mass flow in Extraction to HPP 6 in kg/s

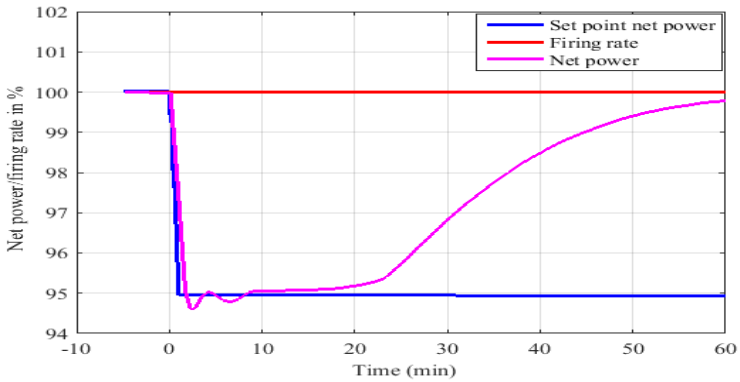

Fig 8 : Analysis of the set point net power, firing rate and net power in%

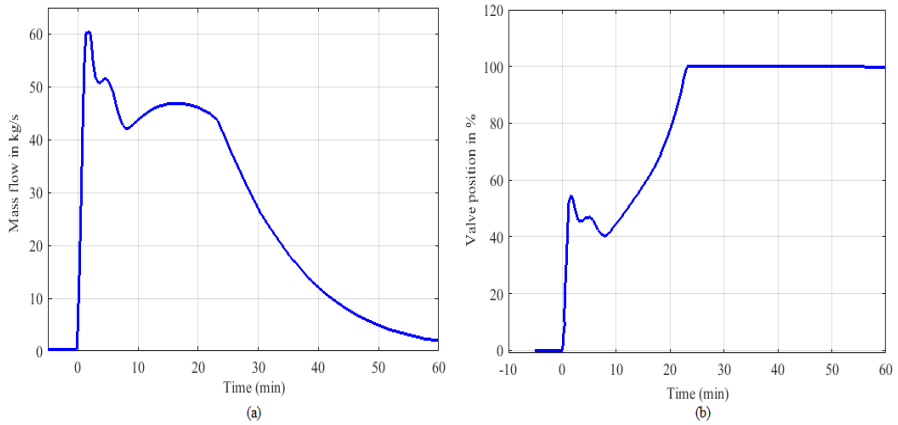

Fig 9: Comparison of (a) inlet mass flow ruths storage in kg/s (b) valve opening position in%

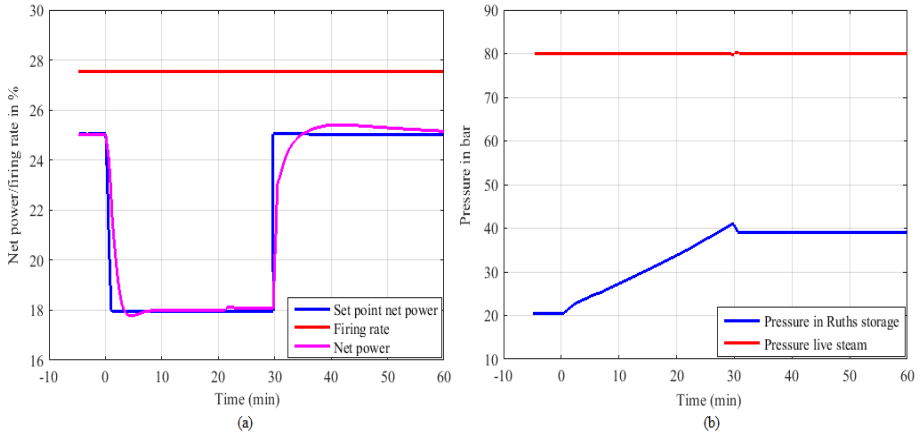

Fig 10: Comparison of (a) Net power firing rate (b) Pressure in bar

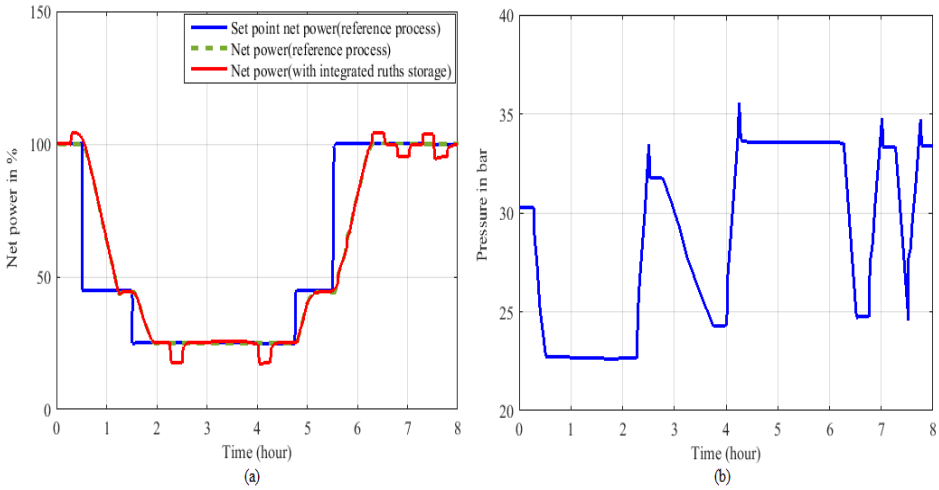

Fig 11: Analysis of (a) Net power in % (b) Pressure in bar

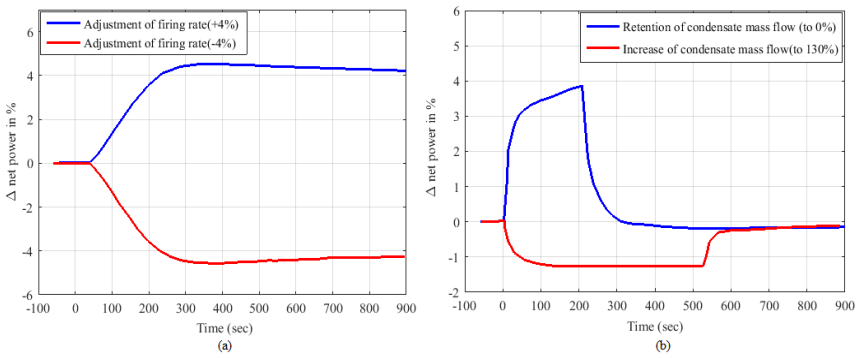

Fig 12: Analyses of Δ net power in % (a) Adjustment firing rate (b) retention &increase of condensate mass flow.

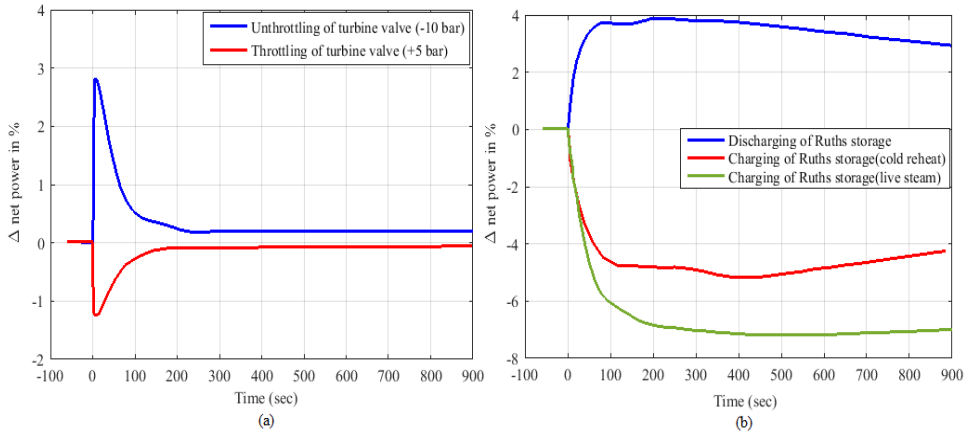

Fig 13: Analysis of (a) Unthrottling & throttling of turbine valve (b) Discharging & charging of Ruths storage.

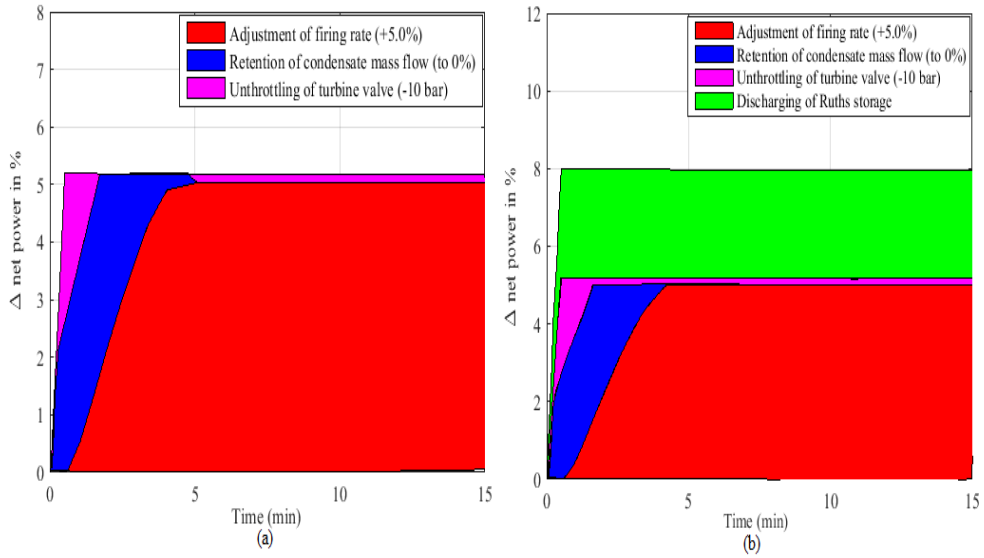

Fig 14: Analysis of change in total power of (a) step responses of typical process-inherent energy storages, (b) supplemented by the integrated Ruths storage

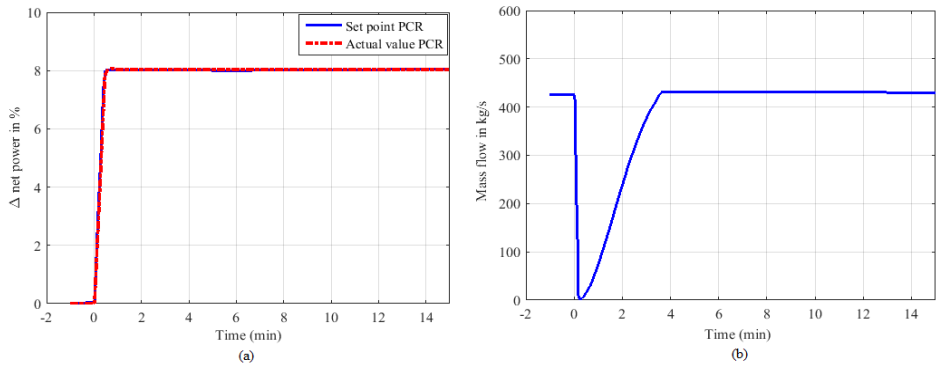

Fig 15: Analysis of (a) Δ net power in% (b) mass flow in kg/s.

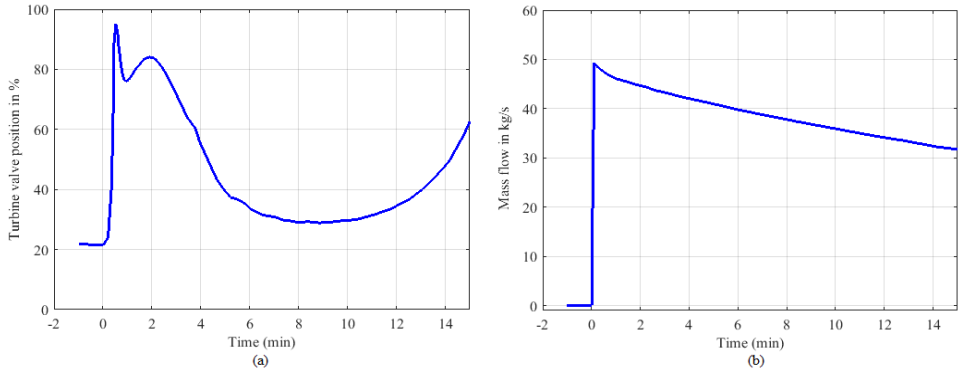

Fig 16: Analysis of (a) turbine valve position in % (b) Mass flow in kg/s.

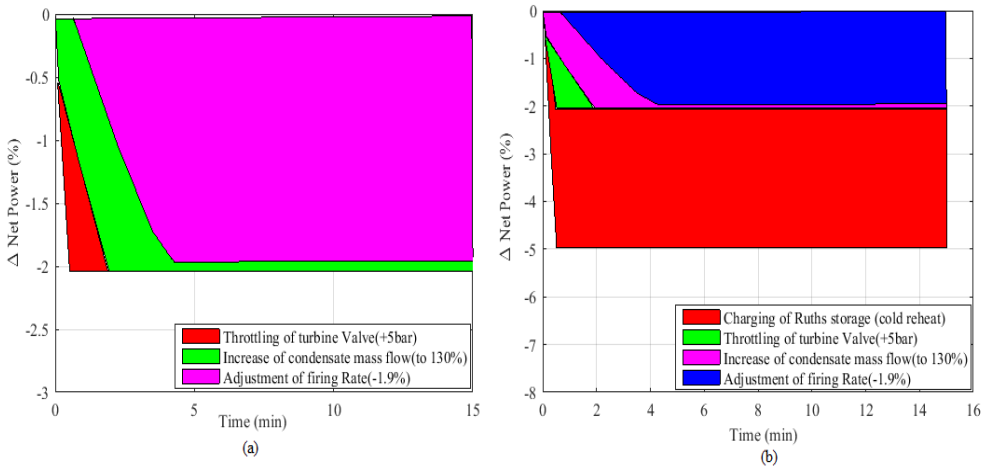

Fig 17: Analysis of (a) maximal possible negative PCR-provision, (b) supplemented by integrated Ruths storage.

Fig 10 shows the comparison of net power firing rate and pressure in bar. Subplot 10(a) depicts the variations in set point net power, firing rate and net power in %. The set point net power starts in -5min at the beginning with 25% and remains constant upto 0min. After that it decreases to 18% in 1min and remains constant till 30min. At end of the cycle it again rises to 25% and remains stable.

The firing rate remains constant in 100% from the beginning to the end at 60min. The net power is at 25% in -5min and remains same upto 0min. In 3min the the value drops to 17.9%. The net power reaches 25.4% in

40min and drops to 25% at the end of the cycle. Subplot 10(b) depicts the variations in pressure in Ruths storage and live stream in bar. The pressure in Ruths storage starts with 20bar in -5min and remains constant upto 0min.

After that it rises to 40bar in 30 min. Then it decreases to 39bar and remains the same till the end of the cycle. The pressure in live steam starts with 80bar and remains constant upto 60min in the end.The analysis of net power and pressure in bar are shown in Fig. 11. Subplot 11(a) depicts the variations in set point net power (reference process), net power (reference process) and net power (with combined ruths-storage).

The set point net power (reference process) starts with 100% in 0hr min and remains constant upto 0.5hr and then drops to 49%. At the time period of 1.5hrs the value is at 25% and remains constant till the time reaches to 4.8hrs. Finally the value reaches 100% and remains constant upto 8hrs. The net power (reference process) starts with 100% in the beginning and remains constant upto 0.5hr. After that it drops to 49.5% in 1.2hr. At the time period of 1.9hrs, the value drops to 25% and remains constant upto 4.7hrs.

Then it rises to 105% in 6.5hrs. The net power (with integrated ruths storage) is at 100% and remains the same till 12.5hrs. After that it slightly varies and decreases to 49% at 1.2hr. In 5.5hrs, the value is at 50% and rises to 105% in 6.2hrs. At the end of the cycle the total power (with combined ruths storage) is at 100%. Subplot 11(b) depicts the pressure in ruths storage in bar. The pressure is at 30 bar in the beginning and remains constant upto 0.4hr.

Then it drops to 22.5bar in 0.5hr and remains constant upto 2.2 hr. The value reaches the maximum of 35.1bar in 4.2hrs. The pressure remains in 33.5bar at end of the cycle in 8hrs. Fig. 12 shows the analyses of Δ net power in % (a) Adjustment firing rate (b) retention &increase of condensate mass flow. Subplot 12(a) depicts the variations in adjustment of firing rate (+4%) and adjustment of firing rate (-4%). The adjustment of firing rate (+4%) starts with 0% from -50sec and remains constant upto 0sec.

After that, end of the cycle, it rises to 4.5% in 300sec and remains stable. The adjustment of firing rate (-4%) is at 0% in the beginning and remains the same till 0 sec. Then it drops to -4.5% in 300sec and remains the same till 900sec. Subplot 12(b) depicts the variations in retention of condensate mass flow (to 0%) and increase of condensate mass flow (to 130%). The retention of condensate mass flow (to 0%) is at 0% in the beginning and remains same till 0sec.

Afterwards it increases to the maximum of 4% in 200sec. At the time of 500sec the value drops to -0.1% and remains stable till end of the cycle. The increase of condensate mass flow (to 130%) starts with 0% in the beginning and drops to -1.2% in 100sec. At end of the cycle the value reaches 0%. The analysis of unthrottling& throttling of turbine valve and discharging & charging of Ruths storage are shown in Fig. 13. Subplot 13(a) depicts the variations in unthrottling of turbine valve (-10 bar) & throttling of turbine valve (+5bar).

The unthrottling of turbine valve (-10 bar) starts with the Δ net power of 0% in the beginning and remains same till 0sec. After that it rises to its maximum Δ net power of 2.9% at 0sec and drops 0.1% at 200sec and remains constant upto the end. The throttling of turbine valve (+5bar) is in 0% of Δ net power at the beginning and drops to -1.1%. After that it reaches to 0% at 200 sec and remains the same upto 900sec.

Subplot 13(b) depicts the variations in discharging & charging of Ruths storage (cold reheat & live steam). The discharging of Ruths storage starts with 0% of Δ net power at the beginning and remains the same till 0sec. After that it rises to 4% in 200 sec. At the end in 900 sec it drops to 3%. The charging of ruths storage (cold reheat) starts with 0% at the beginning and remains constant upto 0sec.

Then it drops to -4.9% at 100 sec and in the end it reaches -4%. Charging of ruths storage (live steam) starts with 0% of Δ net power and remains constant upto 0sec. After that it drops to -7% in 200sec and remains constant till 900sec. Analysis of change in total power of (a) step responses of typical process-inherent energy storages, (b) supplemented by integrated Ruths storage is portrayed in Fig. 14.

Subplot 14(a) shows the variations in adjustment firing rate (+5.0%), retention of condensate mass flow (to 0%) and unthrottling of turbine valve (-10bar).

The adjustment firing rate (+5.0%) starts with 0% of Δ net power and reaches to 4.9% in 4min and remains stable till end of the cycle. Retention of condensate mass flow (to 0%) starts with 0 at the beginning and reaches to 5% of Δ net power in 1min. Then it remains constant upto 5min.Unthrottling of turbine valve (-10bar) starts with Δ net power 0% and increases to 5% in 1min and remains constant upto the end. Subplot 14(b) shows the variations in adjustment firing rate (+5.0%), retention of condensate mass flow (to 0%), unthrottling of turbine valve (-10bar) and discharging of Ruths storage.

Adjustment firing rate (+5.0%) is 5% of Δ net power in 1min and remains the same till the end. Retention of condensate mass flow (to 0%) reaches to 5% of Δ net power in 1min and remains constant till the time period of 5min. In 1min the Unthrottling of turbine valve (-10bar) increases to 5% and remains same upto 15min. The discharging of Ruths storage starts with 0% in the beginning and reaches to the maximum of 6% in Δ net power at the time period of 1min and remains same upto the end.

The analysis of Δ net power in% and mass flow in kg/s are shown in Fig. 15. Subplot 15(a) shows the variations in set point PCR and actual value PCR. The set point PCR starts with 0% of Δ net power in the beginning and remains constant upto 0min. After that it rises to the maximum of 8% and remains stable till the end of the cycle at 15min. The actual value PCR is as same as the set point PCR. Subplot 15(b) shows the variation of condensate mass flow which starts with 425kg/s and remains constant upto 0min. After that it drops to 0% in 0.1sec. Then the mass flow rises to 425 at the time period of 3min and remains same till 15min.

The analysis of turbine valve position and mass flow are shown in Fig. 16. Subplot 16(a) shows the variation of opening turbine valve position which is in 20% at the beginning. The valve position reaches to tits maximum of 99% at the time of 1min. At the end it drops to 60% in 15min. Subplot 16(b) depicts the variation in mass flow at outlet of ruths storage which is in 0kg/sat the beginning and remains constant upto 0min. After that it rises to the maximum of 50kg/s and drops to 32kg/s at the end in 15min.

Fig. 17 shows the analysis of (a) maximal possible negative PCR-provision, (b) supplemented by integrated Ruths storage. Subplot 17(a) depicts the maximal possible negative PCR-provision. The fig shows the variations in throttling of the turbine valve (+5bar), an increase in condensate mass flow (to 130%), and an adjustment in firing rate (-1.9%). Throttling of the turbine valve (+5bar) starts with Δ a net power of 0% initially, drops to -2% in 0.5 minutes, and remains stable. The increase in condensate mass flow (to 130%) starts in 0 minutes with 0% of Δ net power, drops to -2% in 2 minutes, and remains constant up to the end. The adjustment of firing rate (-1.9%) is at 0% in the beginning, decreases to -1.9% at 4 minutes, and remains the same till the time of 15min.

Table 1: Comparative of flexibility-parameters affected by combining TES

Flexibility parameter	Initial state	Potential
Minimal-load	26.0%	19.0%
Maximal-load	101.0%	105.3%
Changeable load capacity with a steady firing ratio	-	+5.3%/16.4MWh$_{el}$ (discharge of thermal energy storage)
		-6.0%/19.6 MWh$_{el}$(charge of thermal energy storage, cold reheat)
		-8.0%/26.1 MWh$_{el}$(charge of thermal energy storage, live steam)
Main control-reserve	±3.1%	±5.0%

Table 2: Comparison between the overall efficiency of the energy systemwith past studies

Study	Thermal Storage Efficiency (%)	Conventional Efficiency (%)
Wang and Song [53]	35.5%	33.9%
Wang et al. [54]	37.2%	34.3%
Ouyang et al. [55]	39.3%	36.8%
Proposed	46.9%	42.5%

Table 1 shows the comparative of flexibility-parameters affected by combining TES. From the table, we can conclude that the net power is very high. Table 2 shows the comparison between the overall efficiency of the energy system with past studies. The overall efficiency is calculated based on the thermal storage efficiency and conventional efficiency.

In the first study by Wang and Song [53], the thermal storage efficiency was found to be 35.5%, while the conventional efficiency was 33.9%. In the second study by Wang et al. [54], the thermal storage efficiency was slightly higher at 37.2%, and the conventional efficiency was 34.3%. The third study by Ouyang et al. [55] reported a thermal storage efficiency of 39.3% and a conventional efficiency of 36.8%. In the proposed study, the thermal storage efficiency is significantly higher at 46.9%, compared to past studies.

The conventional efficiency in the proposed study is also higher at 42.5% compared to past studies. Overall, the proposed study demonstrates improved efficiency in both thermal storage and conventional energy systems compared to the previous studies.

5. Conclusion

In conclusion, this study presents a pioneering method to bolster the load flexibility of CFPPs by combining HTTES through an additional thermodynamic cycle. The goal was to find out if it was possible to add HTTES-assisted extra cycling to the steam-water cycle of regular CFPPs and how that would affect the efficiency of the whole process. Through meticulous analysis of the thermal system and operational mode of an HTTES-assisted CFPP, alongside the utilization of a subcritical CFPP model, the study unequivocally demonstrates that HTTES integration amplifies the load flexibility of CFPPs. Specifically, during periods when the original unit operates at maximum capacity, additional total power output can be achieved. Remarkably, the study's results showcase a thermal storage efficiency of 46.9%, a notable improvement compared to previous research endeavors, while conventional efficiency also registers a commendable enhancement to 42.5%. These findings underscore the considerable potential of HTTES integration in enhancing the efficiency and flexibility of CFPPs. Overall, this study gives a thorough look at how HTTES can be used to improve load flexibility in CFPPs. It is useful information for both researchers and professionals in the power generation field who want to improve the performance and flexibility of CFPPs. Furthermore, the study's outcomes contribute significantly to the advancement of load flexibility technologies and furnish a robust foundation for future research and implementation endeavors. The proposed novel approach, executed using the MATLAB platform, heralds promising prospects for the evolution of CFPPs towards greater efficiency and sustainability in the face of evolving energy dynamics.

Data Availability Declaration

Nil

Funding Specifics

None

References

[1] W. Zappa, M. Junginger and M. van den Broek, Is a 100% renewable European power system feasible by 2050?,*Appl. Energy.*, 233–234 1 2019, 1027–1050.
[2] Z.Liu, D.Guan, D.Crawford-Brown, Q.Zhang, K.He and J.Liu, A low-carbon road map for China, *Nat.* 500, 7461, 143–145, 2013.
[3] H. Ren, W. Zhou, K. Nakagami, W. Gao and Q. Wu, Feasibility assessment of introducing distributed energy resources in urban areas of China, *Appl. Therm. Eng*, 30 16, 2010,2584–2593
[4] Y. Zhou, Evaluation of renewable energy utilization efficiency in buildings with Exergy analysis, *Appl. Therm. Eng*, 137, 1, 2018,430–439
[5] C. Dong, Y. Qi, W. Dong, X. Lu, T. Liu and S. Qian, Decomposing driving factors for wind curtailment under economic new normal in China, Appl. Energy., 217, 2018, 1, pp. 178–188.
[6] J.W. Busby and S. Shidore, Solar federalism: What explains the variation in solar capacity additions by India's states?., Energy Res. Soc. Sci., 71, 1, 2021,101815,
[7] Y. Pamu and P. SVSNDL, An experimental analysis for clay bricks manufacturing with partial replacement of glass wool, *Aust. J. Struct. Eng.*, 1, 1, ,2023,1-16,
[8] Y. Pamu and S. Alugubelli, A comparative study of environmental impacts due to conventional and sustainable concrete, *Mater. Today Proc.*, 1, 1, 2023,1-1,
[9] Y. Wu, L. Fu, S. Zhang and D. Tang, Study on a novel co-operated heat and power system for improving energy efficiency and flexibility of cogeneration plants, *Appl. Therm. Eng*, 163, 1, ,2019,114429.
[10] N. Tang, Y. Zhang, Y. Niu and X. Du, Solar energy curtailment in China: Status quo, reasons and solutions, *Renew. Sust. Energ. Rev*., 97, 1, 2018,509–528
[11] Y. Cai and Y. Aoyama, Fragmented authorities, institutional misalignments, and challenges to renewable energy transition: A case study of wind power curtailment in China, *Energy Res. Soc. Sci..*, 41, 1, 2018, 71–79.
[12] R. Golden and B. Paulos, Curtailment of renewable energy in California and beyond ,*Electr. J.*, 28, 6, 2015,36–50.
[13] L. Bird, D. Lew, M. Milligan, E.M. Carlini, A. Estanqueiro, D. Flynn, E. Gomez-Lazaro, H. Holttinen, N. Menemenlis, A. Orths and P.B. Eriksen, Wind and solar energy curtailment: A review of international experience , *Renew. Sust. Energ. Rev.*,. 65, 1, 2016,577–586.
[14] M. Esteban, J. Portugal-Pereira, B.C. Mclellan, J. Bricker, H. Farzaneh, N. Djalilova, K.N. Ishihara, H.Takagi and V. Roeber, 100% renewable energy system in Japan: Smoothening and ancillary services, *Appl. Energy*., 224, 1, 2018,698–707,
[15] M. Joos and I. Staffell, Short-term integration costs of variable renewable energy: Wind curtailment and balancing in Britain and Germany, *Renew. Sust. Energ. Rev.*, 86, 1, ,2018, 45–65.
[16] T. Mai, R. Wiser, D. Sandor, G. Brinkman, G. Heath, P. Denholm, D.J. Hostick, N. Darghouth, A. Schlosser and K. Strzepek, Renewable Electricity Futures Study. volume 1: Exploration of high-penetration renewable electricity futures 1, 2, 1-1, 2012.
[17] X. Luo, J. Wang, M. Dooner and J. Clarke, Overview of current development in electrical energy storage technologies and the application potential in power system operation, *Appl. Energy*., 137, 1, 511–536, 2015.
[18] A. Olson, R. A. Jones, E. Hart and J. Hargreaves, Renewable curtailment as a power system flexibility resource, Electr. J., 27, 9, 49–61. 2014.
[19] R. Zhai, H. Liu, C. Li, M. Zhao and Y. Yang, Analysis of a solar-aided coal-fired power generation system based on Thermo-Economic Structural theory, *ENG.*, 102, 1, , 375–387 2016.
[20] M. L. Kubik, P. J. Coker and J. F. Barlow, Increasing thermal plant flexibility in a high renewables power system, *Appl. Energy*.,154,1,102–111,2015. https://www.sciencedirect.com/science/article/abs/pii/S0306261915005267
[21] Y. Guo and D. Yu, The influence of interconnection of electric power systems on load characteristic and frequency regulation, *Electr. Power Syst. Res.*, 70, 1, 23–29,2004,

[22] W. Wang, Li L, Long D, Liu J, Zeng D, Cui C, "Improved boiler-turbine coordinated control of 1000 MW power units by introducing condensate throttling," *J. Process Control*, Vol. 50, No. 1, 2017, 11–18.
[23] G. K. Lausterer, Improved maneuverability of power plants for better grid stability, *Control Eng. Pract.,* 6, 12,1549–1557,1998
[24] M. Zhu, X. Wu, J. Shen and K. Lee, Dynamic modeling, validation and analysis of direct air-cooling condenser with integration to the coal-fired power plant for flexible operation, *Energy Convers. Manag.,* 245, 1, 114601. 2021
[25] R. Cao, Y. Lu, D. Yu, Y. Guo, W. Bao, Z. Zhang and C. Yang, A novel approach to improving load flexibility of coal-fired power plant by integrating high temperature thermal energy storage through additional thermodynamic cycle, *Appl. Therm. Eng.*, 173, 1, 115225 2020.
[26] Z. Wang, M. Liu and J. Yan, Flexibility and efficiency co-enhancement of Thermal Power Plant by control strategy improvement considering time varying and detailed boiler heat storage characteristics, *ENG.*, 232, 1 121048 2021.
[27] Z. Wang, M. Liu, Y. Zhao, C. Wang, D. Chong, and J. Yan, "Flexibility and efficiency enhancement for double-reheat coal-fired power plants by control optimization considering boiler heat storage." *ENG.*, 201, 1, ,117594,2020.
[28] H. Wei, Lu, Y., Yang, Y., Zhang, C., He, C., Wu, Y., Li, W. and Zhao, D., Research on influence of steam extraction parameters and operation load on operational flexibility of coal-fired power plant, *Appl. Therm. Eng.*, 195, 1,117226, 2021.
[29] P. Benalcazar, Sizing and optimizing the operation of thermal energy storage units in combined heat and power plants: An integrated modeling approach, *Energy Convers. Manag.,* 242, 1,114255, 2021.
[30] M. Liu, M. Liu, Y. Wang, W. Chen and J. Yan, Thermodynamic optimization of coal-fired combined heat and power (CHP) systems integrated with steam ejectors to achieve heat–power decoupling, *ENG.*, 229, 1, 120707, 2021.
[31] Y. Zhao, C. Wang, M. Liu, D. Chong and J. Yan, Improving operational flexibility by regulating extraction steam of high-pressure heaters on a 660 MW supercritical coal-fired Power Plant: A Dynamic Simulation, *Appl. Energy*, 212, 1, ,1295–1309, 2018
[32] Y. Hu, D.-L. Zeng, J.-Z. Liu, Z. Zhao and Y. Li, Dynamic model for Controller Design of condensate throttling systems, *ISA Trans.*, 58, 1, 622–628, 2015
[33] W. Wang, J. Liu, D. Zeng, Y. Niu and C. Cui, "Modeling for condensate throttling and its application on the flexible load control of power plants," *Appl. Therm. Eng.*, 95, 1, 303–310, 2016
[34] M. De Rosa, M. Carragher and D. P. Finn, Flexibility assessment of a combined heat-power system (CHP) with energy storage under real-time energy price market framework, *Therm. Sci. Eng. Prog.*, 8, 1, 426–438, 2018
[35] T. Nuytten, B. Claessens, K. Paredis, J. Van Bael and D. Six, Flexibility of a combined heat and power system with thermal energy storage for district heating, *Appl. Energy*, 104, 1,583–591, 2013
[36] K. Wang, S. Chen, L. Liu, T. Zhu and Z. Gan, Enhancement of renewable energy penetration through energy storage technologies in a CHP-based energy system for Chongming, China, *ENG.*, 162, 1,988–1002, 2018.
[37] G. Pagliarini and S. Rainieri, Modeling of a thermal energy storage system coupled with combined heat and power generation for the heating requirements of a university campus, *Appl. Therm. Eng.*, 30, 10,1255–1261,2010.
[38] J. Wojcik and J. Wang, Technical feasibility study of thermal energy storage integration into the conventional power plant cycle, *Energies*, 10, 2, 205 , 2017
[39] D. Li and J. Wang, "Study of supercritical power plant integration with high temperature thermal energy storage for flexible operation," *J. Energy Storage*, 20, 1, ,140–152, 2018
[40] M. Richter, G. Oeljeklaus and K. Görner, Improving the load flexibility of coal-fired power plants by the integration of a thermal energy storage, *Appl. Energy,* 236, 1, 607–621. ,2019

[41] B. Arias, An analysis of the operation of a flexible oxy-fired CFB Power Plant integrated with a thermal energy storage system, *International Int. J. Greenh.*, 45, 1, ,172–180, 2016
[42] M. Trojan, D. Taler, P. Dzierwa, J. Taler, K. Kaczmarski, and J. Wrona, The use of pressure hot water storage tanks to improve the energy flexibility of the steam power unit, *ENG*., 173, 1, 926–936. , 2019
[43] J. Bugge, S. Kjær and R. Blum, High-efficiency coal-fired power plants development and perspectives, *ENG.*, 31, 10–11,1437–1445. ,2006
[44] W. H. Yeo, A.T. Fry, J. Purbolaksono, S. Ramesh, J.I. Inayat-Hussain, H.L. Liew and M. Hamdi, Oxide scale growth and presumed exfoliation in a 700°C or higher steam condition: A simulation study for future operations of ultra-supercritical power plants, *J. Supercrit. Fluids*, 92, 1 , ,215–222. 2014
[45] F. Abe, Research and development of heat-resistant materials for advanced USC power plants with steam temperatures of 700 °C and above, *Eng.*, 1, 2,.,211–224. 2015
[46] S. Kuravi, J. Trahan, D. Y. Goswami, M. M. Rahman and E. K. Stefanakos, Thermal Energy Storage Technologies and systems for concentrating solar power plants, *Prog. Energy Combust. Sci.*, 39, 4,285–319. , 2013
[47] D. K. Sarkar, Codes and standards for power plant design and Operation, *Thermal Power Plant*, 1, 1, ,523–538. 2015
[48] F. Alobaid, N. Mertens, R. Starkloff, T. Lanz, C. Heinze and B. Epple. Progress in dynamic simulation of Thermal power plants, *Prog. Energy Combust. Sci.*, 59, 1, 79–162 , 2017
[49] J. Li, Y. Zhang, Y. Tian, W. Cheng, J. Yang, D. Xu, Y. Wang, K. Xie and A.Y. Ku Reduction of carbon emissions from China's coal-fired power industry: Insights from the province-level data, *J. Clean. Prod.*, 242, 1,118518, 2020
[50] S.Y. Pan, S.W. Snyder, , A.I. Packman, Y.J. Lin and P.C. Chiang, Cooling water use in thermoelectric power generation and its associated challenges for addressing water-energy nexus, *Water-Energy Nexus*, 1, 1,26–41. , 2018
[51] Y. Shang, J. Wang, J. Liu, D. Jiang, J. Zhai and S. Jiang, Suitability analysis of China's energy development strategy in the context of water resource management, *ENG*., 96, 1, 286–293, 2016.
[52] J. G. Bustamante, A. S. Rattner and S. Garimella, Achieving near-water-cooled power plant performance with air-cooled condensers, *Appl. Therm. Eng.*, 105, 1, 362–371, 2016.
[53] C. Wang and Song, J. Performance assessment of the novel coal-fired combined heat and power plant integrating with flexibility renovations. *ENG*. 263, 1, 125886, 2023.
[54] C. Wang, J. Song, W. Zheng, L. Zhu, J. Guo and W. Wang, "Integration of compressed air energy storage into combined heat and power plants: A solution to flexibility and economy." *Energy Convers. Manag.*, 290, 1, 117215. 2023.
[55] T. Ouyang, P. Qin, S. Xie, X. Tan and M. Pan, "Flexible dispatch strategy of purchasing-selling electricity for coal-fired power plant based on compressed air energy storage." *ENG*. 267, 1, 126578. 2023